Advances on a Hall thruster hybrid code

IEPC-2007-066

Presented at the 30th International Electric Propulsion Conference, Florence, Italy
September 17-20, 2007

I. Maqueda,* D. Escobar,† and E. Ahedo ‡
Universidad Politécnica de Madrid, Madrid 28040, Spain

A hybrid code is used to simulate the plasma response of a laboratory Hall thruster. Simulations are compared with experimental data in order to identify relevant differences and ways to improve the plasma models. Turbulence diffusion is briefly commented. An alternative model for the interaction of the plasma with ceramic walls is proposed, which yields temperature profiles that agree rather well with experimental ones. A new model for injection of electrons into the discharge is presented, with the aim of simulating the near-plume region and providing a good coupling with plume codes.

I. Simulation of a laboratory thruster

The two-dimensional hybrid code HPHall-2[1,2] is being used for simulating a 2kW thruster designed by the Princeton Plasma Physics Laboratory (PPPL).[3] First simulations on this thruster were presented last year for a mass flow of 5mg/s in Ref. 4. Sketches of the geometry, magnetic field, and numerical meshes can be found there.

Figure 1 depicts the comparison between experiments and simulations for a mass flow of 1.9mg/s and two discharge voltages. The sheath case 1, defined below, was assumed for plasma-wall interaction. This low mass-flow case presented problems of numerical convergence that we just solved recently. A strategy based in fixing the discharge power, P_d, instead of the discharge voltage, V_d, has turned out to be much more stable numerically and is used throughout this paper.

There are three main features where simulation and experimental results differ and, hence, further theoretical research is required. Simulations yield (1) lower peak temperatures, (2) gentler potential profiles (i.e. lower axial electric fields), and (3) lower efficiencies. Differences in temperature profiles are mainly due to the plasma-wall interaction model implemented in the code. This issue is afforded in the next section and affects, to a certain degree, the two other differences.

With respect to the second issue, i.e. too gentle potential profiles, steeper profiles can be recovered if Bohm-type turbulence is considered to be 'non-uniform' along the plasma discharge.[5,6] The physical justification for certain turbulence models[7,8] is the demonstrated turbulence suppression in fusion plasmas in the region of strong $\boldsymbol{E}\times\boldsymbol{B}$ shear.[9] However, the plasma in a Hall thruster presents important differences with the plasma in a tokamak plasma edge and, to our knowledge, there are not equivalent experiments and theories demonstrating turbulence quenching in Hall thruster discharges. In these circumstances the choice of a particular expression for the turbulent term in a Hall thruster model is an *ad hoc* assumption, aimed to replicate a particular potential profile. Indeed, a bibliographical review reveals a contradicting variety of choices of the turbulence parameter.

As our particular contribution to turbulence tailoring in simulation codes, Fig. 2 plots the effect of modifying the turbulence function in the simulations of the PPPL thruster. In general, turbulence is modelled as a contribution $\nu_{turb}=\alpha_{turb}\omega_e$ to the electron collision frequency [see Eq.(6) below] with ω_e the electron gyrofrequency. More correct physically is to see turbulence as an additional force, $F_{\theta,turb}$ that balances the magnetic and resistive azimuthal forces, $F_{\theta,mag}=-en_eu_{\perp e}B$ and $F_{\theta,res}=-m_en_eu_{\theta e}(\nu_{en}+\nu_{wm})$, respectively.[10–12] Fig. 2 shows that a reduction of α_{turb} of 5 times in the region of maximum electric field

*Student, Escuela Técnica Superior de Ingenieros Aeronáuticos(ETSIA).
†Graduate student, ETSIA.
‡Professor, ETSIA, eduardo.ahedo@upm.es.

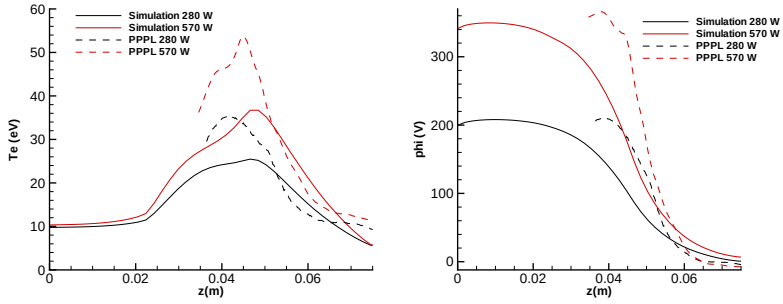

Figure 1. Comparison of experimental results with first simulations of the PPPL 2-kW thruster for two discharge powers and a mass flow of 1.9mg/s. The experimental propellant utilizations are $\eta_u \sim$ 74% for the two cases. The simulations yield η_u =50% and 58% for 280W and 570W, respectively.

(case 3) is able to recover the experimental values of about 30-35 kV/m. (The axial shift in the position of the peak electric field between simulations and experiments is surely due to phenomena inside the chamber.)

Only one observation is worth to be added for this subject and case 3. The ratio $F_{\theta,turb}$ indicates that turbulence *is not suppressed* in the region where α_{turb} is minimum. In fact, in that region the turbulence force still amounts to a 60% of the magnetic force and its shape presents only a small depression.

II. Changes on the plasma-wall model

HPHall-2 assumes a quasineutral plasma except for Debye sheaths tied to the lateral walls and the anode. The model currently implemented for the plasma interaction with the lateral, ceramic walls is that of Ahedo,[13] which assumes quick thermalization of secondary electron emission(SEE) and primary electrons, into a unique electron population in the bulk of the plasma. However, an estimate of the electron thermalization frequency (based on probable collisions and instabilities) seem not to support 'total thermalization' of the electron velocity distribution function(VDF). On the one hand, several authors suggest that the tail of primary electrons collected by the lateral walls remains depleted partially.[14–17] On the other hand, the beam of secondary electrons would not disappear as fast as the total thermalization model assumes. Ahedo and Parra[18] and Sydorenko et. al.[19] showed that the persistence of a fraction of the SEE beams as independent populations from the primary distribution, can reduce largely the electron energy losses to the wall.

Ahedo and dePablo[20] have built a sheath model that takes into account (i) the partial depletion of primary electrons, (ii) the presence of beams of true-secondary electrons, and (iii) the backscattering of primary electrons at the wall. A hypothesis of the model is that primary and secondary electrons thermalize at the same rate (i.e. with the same mean-free-path). The model yields similar results for electron energy losses than Ahedo and Parra, but lower sheath potential falls (which reduces wall erosion by ion impact) because of the depletion of the primary VDF tail. Electron backscattering further reduces the sheath potential fall and energy losses.

There are two difficulties for the implementation of the Ahedo-dePablo model in HPHall-2. First, the electron model for the quasineutral plasma is not prepared at all to include SEE beams as independent electron populations. Second, there are reasons that suggest that thermalization of secondary and primary electrons take place at a different rate. For instance, Sydorenko et al.[21] showed that the two-stream instability can heat quickly the SEE beams. On-going research from our part suggests that (disregarding the instability) the SEE beams can get trapped within the plasma bulk by magnetic effects.

These facts have leaded us to implement provisionally in the code a sheath model (or subcode) that is intermediate between those of Refs. 13 and 20. The model, detailed in the Appendix, takes into account the partial depletion of primary electrons and the presence of backscattered primary electrons, but assumes that the beams of true-secondary electrons get thermalized quickly. The inputs from the *electron subcode* to the *sheath subcode* are the electron temperature at the sheath edge Q, T_{eQ}, the fraction σ of the tail of collected primary electrons that is replenished, the expressions of the SEE yields for true-secondary (hereafter called beam) and reflected electrons

$$\delta_{sb}(E) = E/E_b, \qquad \delta_{sr}(E) = \delta_0 \exp(-E/E_r), \tag{1}$$

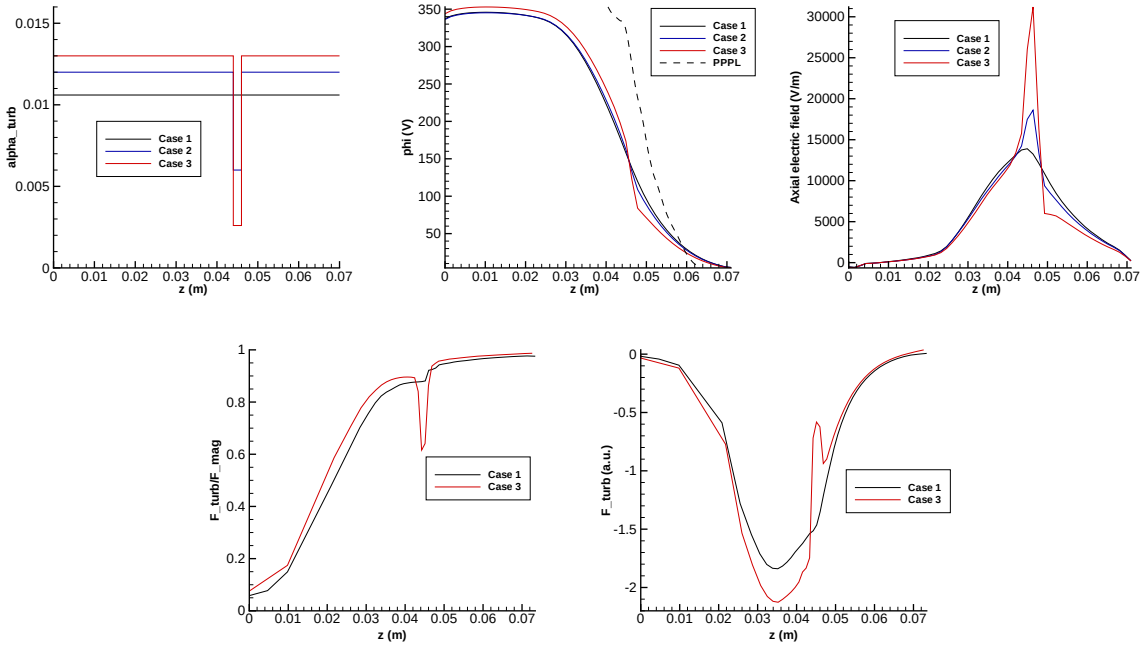

Figure 2. Influence of the turbulence function α_{turb} on the plasma response for 570W and 1.9mg/s.

respectively (with E the energy of the impacting electron), and the emission temperature T_2 of beam electrons. The outputs from the sheath subcode to the electron subcode are (1) the sheath potential fall ϕ_{WQ}, and (2)-(3) dimensionless parameters

$$g_{pQ}/g_{iQ} \quad \text{and} q_{eQ}/(T_{eQ}g_{iQ}) \tag{2}$$

for the flux of primary electrons to the wall, g_{pQ}, and the net flux of electron energy to the sheath, q_{eQ}; eg_{iQ} is the ion current density, known from the PIC subcode.

Figure 3 plots electron energy fluxes at points Q and W and the sheath potential fall for three cases of tail replenishment and wall backscattering, in terms of T_{eQ}. In the three cases $\delta_{sb}(E) + \delta_{sr}(E)$ yields 1 for the same cross-over energy, $E = 47$eV. The role of tail depletion ($\sigma < 1$) and electron backscattering ($\delta_0 > 0$) is different for the 'normal' regime and the charge-saturated regime(CSR). First, within the normal regime, these parameters modify the sheath potential fall *but do not affect* the energy losses to the wall. Second, these parameters affect the location of the charge-saturation limit(CSL) and, as a consequence, they can modify largely the (high) energy losses of the charge-saturation regime(CSR).

Figure 4 shows the plasma response for the sheath case 3 of Fig.4 and compares it to case 1 (the same than in Fig.1) and to experimental results. It is shown that the new plasma-wall model adjusts much better the experimental temperature profile. Also the new propellant utilization of case 3 approaches well the experimental one. The thrust efficiency increases from 20% in case 1 to 30% in case 3. There are no significant variations on the potential profile. The increase in plasma density from case 1 to 3 is due to the higher η_u. This increases the the ion current to wall, j_{iW}, by a factor of $\sim$2. However, the electron energy flux to the wall, q_{eW} decreases by a factor of $\sim$5. This is due to the much lower value of the primary electron flux at the CSR for case 3, $\sim$10 times lower than for case 1, Fig.3. Results for case 2 (not shown here) are closer to case 1 than 3, which means that the key feature for the reduction of wall losses and the good adjustment of the peak temperature is that the tail of wall-collected primary electrons is partially depleted.

III. A volumetric cathode model

In previous sections, the code uses a 'boundary cathode' model, where the near-plume boundary of the simulation domain acts as the neutralization surface, Fig. 5. A backwards electron current I_{eC} is injected

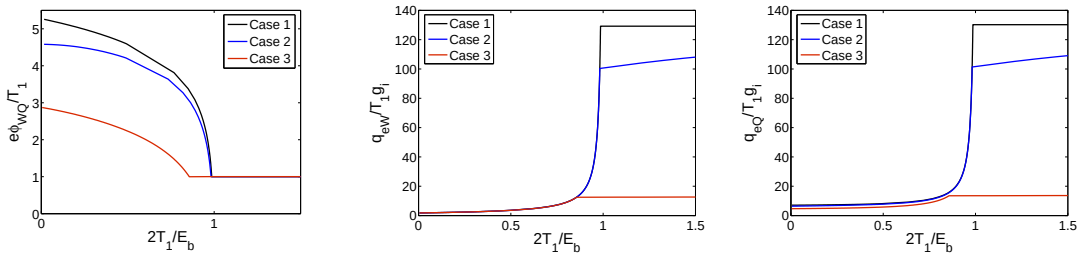

Figure 3. Energy fluxes and sheath potential in terms of the electron temperature for different conditions of the primary VDF tail and electron backscattering at the wall. Case 1: $\sigma = 1$, $E_b = 47\mathbf{eV}$, $\delta_0 = 0$; **Case 2:** $\sigma = 1$, $E_b = E_r = 61\mathbf{eV}$, $\delta_0 = 0.5$; **Case 3:** $\sigma = 0.1$, $E_b = E_r = 61\mathbf{eV}$, $\delta_0 = 0.5$.

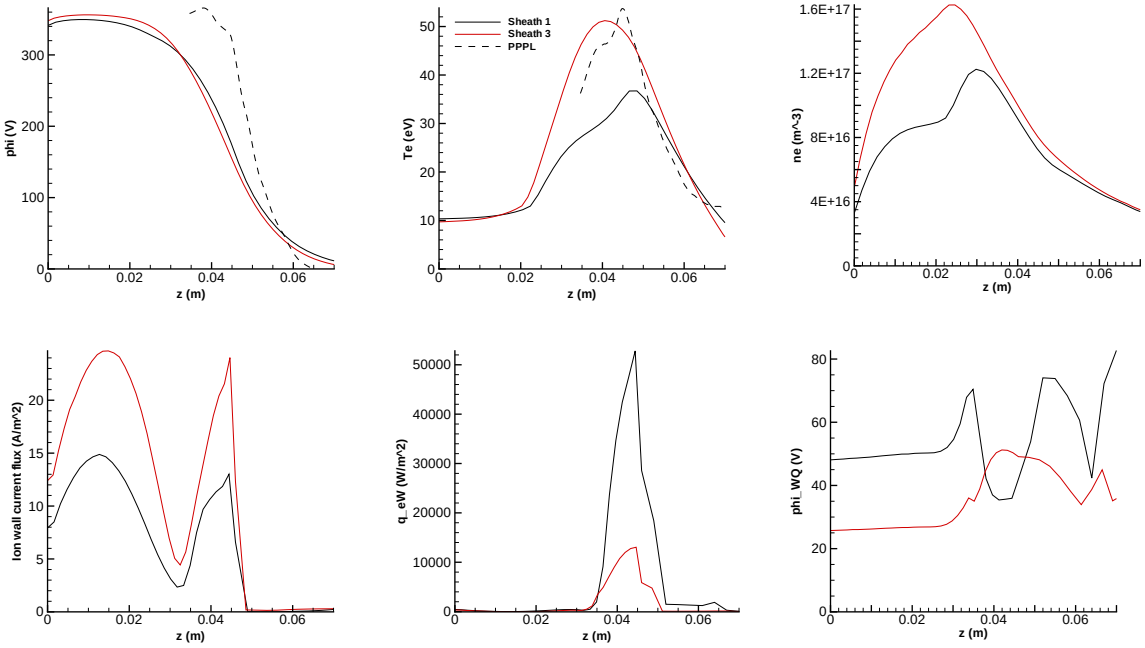

Figure 4. Plasma response of the PPPL thruster for sheath cases 1 and 3 of previous figure, 570W and 1.9mg/s. Case 1 is the same one of Fig.1 (i.e. $\eta_u = 58\%$**). Propellant utilization for case 3 is 69%.**

there and the cathode reference potential is placed at a point of this boundary too. Hence, the code cannot simulate the plasma response across and beyond the region of electron injection.

A first attempt to place the electron injection inside the simulation domain was the 'wall cathode' reported in Ref.,[22] where the electron injector is placed in a small section of the the external wall. A new electron model[23] implemented recently admits the electron exchange through intermediate electrodes placed at the lateral walls of the thruster. The new model was envisaged to study thrusters with two-stages or internal segmented electrodes, but was easily adapted to simulate a 'wall cathode'. Figure 6 sketches this model. An electrical current equal to the discharge current I_d through the external circuit is injected into the plasma domain through an annular cathode, placed on the outer external wall. The surface of the cathode ring and I_d define the current density j_W at the cathode surface. An appropriate sheath model for high emission electrodes[24] determines the boundary conditions needed by the quasineutral code. The injected electron current spreads quickly along the magnetic lines intersecting the cathode. The electric current I at the near-plume boundary of the simulation domain is set to zero, which ensures the neutralization of the ion beam downstream. Figure 6 recovers simulation results for a SPT-100 type of thruster. Observe, at the cathode location, the change on the electron current I_e and the minimum of the electric potential. This is due to the electric forces needed to drive magnetized electrons out of the injection layer. The Joule heating associated to these electric forces heats the electrons fluid. In spite of the success of implementation of the

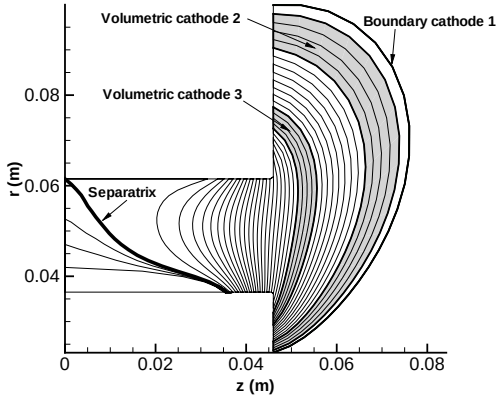

Figure 5. Boundary and volumetric cathode models. The shadowed region is the electron-injection region.

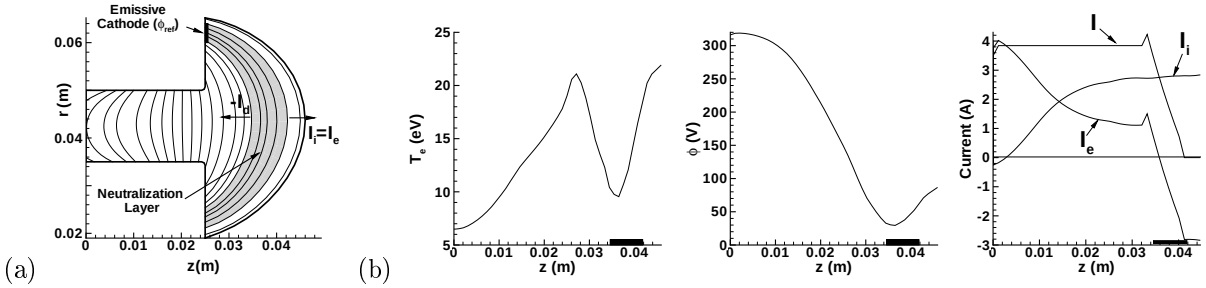

Figure 6. 'Wall cathode' model and plasma response, taken from Ref.22. The cathode is placed at the outer wall and injected electrons spread quickly into the shadowed region.

'wall cathode' model, convergence problems have been detected frequently in simulations. We found out that one important source of instability in the numerical integration lies on strong oscillations of current and potential in the plasma-cathode model. Whereas work is in progress on solving these issues, a second cathode model has been designed.

As in the 'wall cathode' model, the 'volumetric cathode' model injects electrons in a region bounded by two magnetic lines. A point of this region is used as 'cathode reference potential' and no plasma-cathode model is needed. Hence, the 'volumetric cathode' model is simpler to implement and should suffer less from numerical instabilities. The volumetric cathode requires new source terms in the particle and energy equations for electrons:

$$\frac{\partial n_e}{\partial t} + \nabla \cdot n_e \boldsymbol{u}_e = \dot{n}_{ion} + n_e \nu_{cat} \tag{3}$$

$$\frac{\partial}{\partial t}\left(\frac{3}{2} n_e T_e + \frac{m_e u_e^2}{2} n_e\right) + \nabla \cdot \left(\frac{5}{2} T_e n_e \boldsymbol{u}_e + \frac{m_e u_e^2}{2} \boldsymbol{g}_e + \boldsymbol{q}_e\right) = -e n_e \boldsymbol{u}_e \cdot \boldsymbol{E} - \dot{Q}_{ion} + \frac{3}{2} T_{cat} n_e \nu_{cat} \tag{4}$$

Here: most variable names are conventional or obvious; $\dot{n}_{ion}$ is the ionization particle source, $\dot{Q}_{ion}$ is the ionization (plus radiation) energy sink; $n_e \nu_{cat}$ models the cathodic electron source, with $\nu_{cat} = 0$ outside the injection region and constant in the injection region; and T_{cat} is the electron temperature at injection.

A convenient, alternative equation to (8) is the current conservation equation

$$\nabla \cdot (e n_e \boldsymbol{u}_e - \boldsymbol{j}_i) = e n_e \nu_{cat}, \tag{5}$$

where the ion current $\boldsymbol{j}_i$ (with contributions of singly-charged and doubly-charged electrons) is, in HPHall, an input to the electron subcode from the particle-in-cell (PIC) subcode.

The volumetric injection of unmagnetized electrons introduces an extra collisional effect in the effective collision frequency, which takes the form

$$\nu_e = \nu_{en} + \nu_{ion} + \nu_{turb} + \nu_{wm} + \nu_{cat}, \tag{6}$$

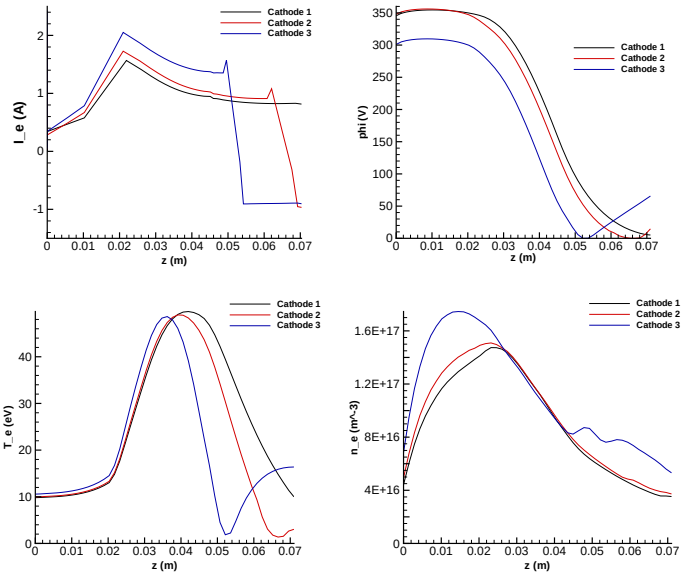

Figure 7. Plasma response at the channel median for the boundary cathode model and the two volumetric cathodes of Fig. 5, for $P_d = 570W$.

with contributions from electro-neutral collisions, ionization, turbulence, wall collisionality (ν_{wm}), and injected electrons (ν_{cat}). The physical basis for this last contribution is the same than for wall collisionality: electrons are injected without any $\boldsymbol{E} \times \boldsymbol{B}$ azimuthal drift.

Figure 5 plots the two 'volumetric cathode' cases that have been simulated. Cathode 3 is mainly an exercise meant to check whether the plasma response is satisfactory downstream of the cathode position.(To move the cathode position inwards is much quicker that to extend the simulation domain into the plume region and re-initiate plasma simulations.) Figure 7 compares profiles at the channel median for the three cases of Fig.5. Observe the change of sign of the electron current I_e at the injection region (and the reduction of the electron current in the near-anode region, after crossing the magnetic separatrix, Fig.5). The similarity of behavior with the 'wall-cathode' model of Fig.6 favors the simpler 'volume-cathode' model, at least while convergence issues with the first one are solved. We expect that the extension of the simulation domain downstream to a region where the magnetic field is negligible, would correct the plasma profiles in the near-plume.

Figure 8 shows 2D maps of the potential profile and the Hall parameter for cathodes 1 and 3. For the Hall parameter of cathode 3, observe: (a) the sharp change at the chamber exit due to the change in wall-collisionality, ν_{wm}, and (b) the shade of volumetric-cathode region provoked by $\nu_{cat} \neq 0$. Figure 9 depicts the different contributions to the electron collision frequency and to the electron energy equation. Observe that turbulence diffusion dominates electron transport except near the anode where electron-neutral collisions are dominant.

IV. Conclusion

A plasma-wall model with partial depletion of the tail of wall-collected primary electrons, implemented in a 2D hybrid code, reproduces very promisingly the experimental peak temperatures and performances of a laboratory Hall thruster.

The implementation of a volumetric cathode model is going to allow the plasma simulation beyond the electron injection region.

Physical phenomena explaining the large peak electric fields found in experiments require further research.

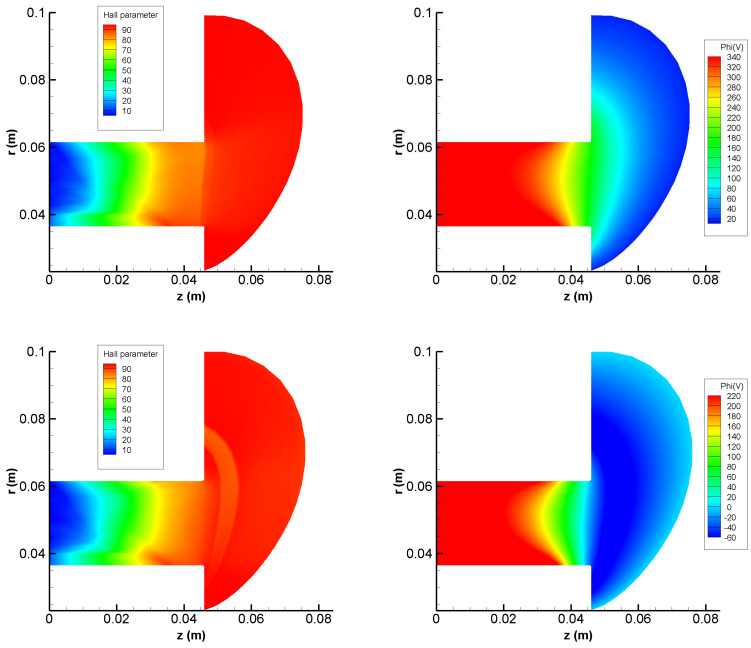

Figure 8. Two-dimensional maps of the Hall parameter and the electric potential for cathodes 1 (up) and 3 (down) of Fig. 5.

Acknowledgments

This work was sponsored by the Ministerio de Educación y Ciencia of Spain, under Project ESP2004-03093. The authors are indebted to Y. Raitses and N. Fisch for the submission of data of the PPPL thruster and fruitful discussions.

V. Appendix: Derivation of the sheath model

We follow here the model of Ref.[20] except for total thermalization of true-secondary electrons. We assume a SEE yield of the form

$$\delta_s = \delta_{sb} + \delta_{sr}, \qquad \delta_{sb}(E) = E/E_b, \qquad \delta_{sr}(E) = \delta_0 \exp(-E/E_r), \tag{7}$$

where δ_{sr} and δ_{sb} correspond to elastically-reflected primary electrons and true-secondary (or beam) electrons, respectively. Let ϕ_{WQ} be the potential fall across the collisionless Debye sheath, which must be determined, and $v_{WQ} = \sqrt{2e\phi_{WQ}/m_e}$. The VDF for primary electrons p at the sheath edge Q is assumed of the form

$$f_{pQ}(v_r, v_\perp) = f_1(v) \times \begin{cases} \delta_{sr}\sigma_1, & v_r < -v_{WQ}, \\ 1, & |v_r| < v_{WQ}, \\ \sigma_1, & v_r > v_{WQ}, \end{cases} \tag{8}$$

Here:

$$f_1(v) = n_1 \left(\frac{m_e}{2\pi T_1}\right)^{3/2} \exp\left(-\frac{m_e v^2}{2T_1}\right), \tag{9}$$

with n_1 and T_1 to be determined; and

$$\sigma_1(\delta_{sr}, \sigma) = \frac{\sigma}{1-(1-\sigma)\delta_{sr}}, \tag{10}$$

with σ the thermalization fraction of the VDF tail.

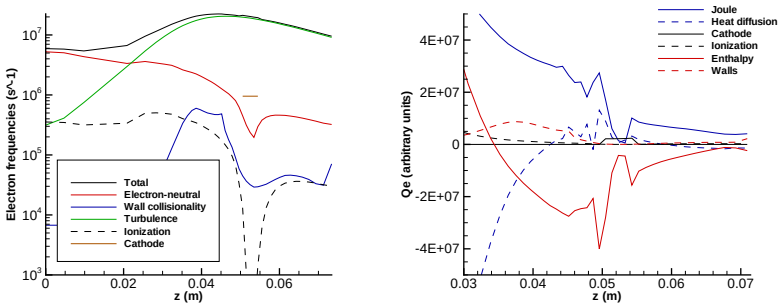

Figure 9. (Left) Contributions to the electron collision frequency. (Right) Contributions to the electron energy equation.

The VDF for beam electrons b at the sheath edge Q (assuming their quick thermalization in the plasma bulk) is

$$f_{bQ}(v) = g_{bQ}\sqrt{\frac{2\pi m_e}{T_2}}\left(\frac{m_e}{2\pi T_2}\right)^{3/2}\exp\left(-\frac{m_e v^2 + e\phi_{WQ}}{2T_2}\right)H\left(-v - v_{WQ}\right) \tag{11}$$

with g_{bQ} their flux, T_2 the emission temperature, and H the Heaviside step function. The flux of beam electrons satisfies

$$g_{bQ} = \tilde{\delta}_{sb}(T_1)g_{pQ}, \qquad \tilde{\delta}_{sb} = 2T_1/E_b. \tag{12}$$

Imposing that the electrical current to the wall is zero, the net flux of primary electron g_{pQ} satisfies

$$\frac{g_{pQ}}{g_{iQ}} = \frac{1}{1-\tilde{\delta}_{sb}}. \tag{13}$$

where $g_{iQ} = j_{iQ}/e$ is the ion current (in particle units) in the sheath provided by the PIC subcode. Hence, the last two equations determine the fluxes of primary and beam electrons in terms of T_1, wall properties, σ, and the ion current. The net flux of electron energy into wall is

$$q_{neW} = 2T_1 g_{pQ} - 2T_2 g_{bQ} = \frac{2T_1 g_{iQ}}{1-\tilde{\delta}_{sb}}\left(1 - 2\frac{T_2}{E_b}\right) \tag{14}$$

where $2T_2 \ll E_b$ reduces the energy flux in a 10% typically.

From f_{pQ}, the net flux of primary electrons into sheath and wall is

$$g_{pQ} = (1-\tilde{\delta}_{sr})\tilde{\sigma}_1 \mathrm{e}^{-\hat{\phi}_{WQ}} n_1\sqrt{T_1/2\pi m_e}, \tag{15}$$

with

$$\tilde{\delta}_{sr}(T_1) = \frac{\delta_0}{(1+T_1/E_r)^2} \tag{16}$$

an approximate value of δ_{sr}, averaged over the VDF, and $\tilde{\sigma}_1 = \sigma_1(\tilde{\delta}_{sr}, \sigma)$.

Solving Eq.(15) for the sheath potential fall,

$$\hat{\phi}_{WQ} \equiv \frac{e\phi_{WQ}}{T_1} = \ln\sqrt{\frac{m_i}{2\pi m_e}} + \ln\left[(1-\tilde{\delta}_{sb})(1-\tilde{\delta}_{sr})\tilde{\sigma}_1\right] + \ln\frac{n_1\sqrt{T_1/m_i}}{g_{iQ}}. \tag{17}$$

The first term of the RHS is large, ~ 200 for xenon. The second term is negative and reduces substantially the sheath fall when the argument of the logarithm is very small (i.e. for true-secondary emission near 100% or for low thermalization). The last term requires is always small and will be neglected hereafter. The electron energy flux at the sheath edge Q satisfies

$$q_{neQ} = q_{neW} + e\phi_{WQ}g_{iQ}. \tag{18}$$

The 'normal' regime of the sheath described above ends at the charge saturation limit (CSL), defined by the condition of zero electric field at the wall or, equivalently, zero total electric charge in the sheath

$$\int_W^Q \left[en_p(\phi) + en_b(\phi)\right] d\phi = \int_W^Q \rho_i(\phi) d\phi, \tag{19}$$

with $\rho_i(\phi)$ the ion electric charge in the sheath. An analytical expression for the left-hand side is immediate, but $\rho_i(\phi)$ requires to know, from the PIC subcode, the distribution function of singly-charged and doubly-charged ions at the sheath edge, and then compute the right-hand side in each timestep and for each simulation node, which is very time-consuming. For present purposes, focused on a first evaluation of the effects of $\sigma < 1$ and $\delta_{sr} > 0$ on the energy losses at laterals walls and thruster performances, we set arbitrarily the CSL condition at a given value of the dimensionless potential fall, that is we fix $\hat{\phi}^*_{WQ}$ (superscript * is used for the CSL magnitudes). Previous studies,[13,18,20] based on assuming a quasi-monoenergetic population of singly-charged ions, yield $\hat{\phi}^*_{WQ} \sim 0.5 - 1$.

Finally, the temperature T_1 must be related to the temperature T_{eQ} of the unique electron population used in the bulk, quasineutral region. Since the density of beam electrons is small at the sheath edge and we are assuming that these electrons thermalize quickly with the bulk electron population bulk region, we will derive T_{eQ} only from the contribution of f_{pQ}, Eq.(8). This VDF yields different temperatures in the directions parallel and perpendicular to the wall. Clearly, the wall-parallel temperature is T_1. The wall-perpendicular (subscript n) energy of primary electrons at Q is

$$\int \frac{1}{2} m_e v_n^2 f_{pQ} d^3v \equiv \mathcal{E}_{npQ} = n_{pQ} \left(\frac{1}{2} m_e u_{npQ}^2 + \frac{1}{2} T_{npQ} \right) \tag{20}$$

with $u_{npQ} = g_{pQ}/n_{pQ}$ a macroscopic electron velocity. Then, the wall-perpendicular temperature T_{npQ} satisfies

$$\frac{T_{npQ}}{T_1} \equiv \hat{T}_{npQ} = \frac{2\hat{\mathcal{E}}_{npQ}}{\hat{n}_{pQ}} - \frac{1}{2\pi} \left[\frac{(1-\tilde{\delta}_{sr})\tilde{\sigma}_1 \mathrm{e}^{-\hat{\phi}_{WQ}}}{n_{pQ}} \right]^2 \tag{21}$$

with

$$2\hat{\mathcal{E}}_{npQ} = 1 - \left(1 - \tilde{\sigma}_1 \frac{1+\tilde{\delta}_{sr}}{2} \right) \left(2 \frac{\hat{\phi}_{WQ}^{1/2}}{\pi^{1/2}} \mathrm{e}^{-\hat{\phi}_{WQ}} + \mathrm{erfc} \hat{\phi}_{WQ}^{1/2} \right), \tag{22}$$

and

$$\hat{n}_{pQ} \equiv \frac{n_{pQ}}{n_1} = 1 - \left(1 - \tilde{\sigma}_1 \frac{1+\tilde{\delta}_{sr}}{2} \right) \mathrm{erfc} \hat{\phi}_{WQ}^{1/2}. \tag{23}$$

Then, the appropriate relation between T_1 and the temperature T_{eQ} is

$$T_1 = T_{eQ} \frac{3}{2 + \hat{T}_{npQ}}. \tag{24}$$

Computations show that $T_{eQ}/T_1 \sim 0.85 - 1$. Notice that T_{eQ} and not T_1 is the actual input parameter to compute sheath magnitudes.

References

[1] J. M. Fife, *Hybrid-PIC Modeling and Electrostatic Probe Survey of Hall Thrusters*, PhD thesis, Massachusetts Institute of Technology, 1998.

[2] F. Parra, E. Ahedo, M. Fife, and M. Martínez-Sánchez, Journal of Applied Physics **100**, 023304 (2006).

[3] Y. Raitses, D. Staack, L. Dorf, and N. Fisch, Experimental study of acceleration region in a 2kW Hall thruster, in *39th Joint Propulsion Conference, Huntsville, AL*, AIAA 2003-5153, American Institute of Aeronautics and Astronautics,Washington, DC, 2003.

[4] E. Ahedo, I. Maqueda, A. Antón, Y. Raitses, and N. Fisch, Numerical simulations of a 2kW Hall thruster, in *42th Joint Propulsion Conference, Sacramento, CA*, AIAA-2006-4655, American Institute of Aeronautics and Astronautics,Washington, DC, 2006.

[5] G. Hagelaar, J. Bareilles, L. Garrigues, and J. Boeuf, Journal of Applied Physics **93**, 67 (2003).

[6] J. Koo and I. Boyd, Physics Of Plasmas **13**, 033501 (2006).

[7]M.Cappelli, N. Meezan, and N. Gascon, Transport Physics in Hall Plasma Thrusters, in , AIAA 2002-0485, American Institute of Aeronautics and Astronautics, Washington DC, 2002.

[8]J. Fox, A. Batishcheva, O. V. Batishchev, and M.Martinez-Sanchez, Adaptively Meshed Fully-Kinetic PIC-Vlasov Model For Near Vacuum Hall Thrusters, in *42th Joint Propulsion Conference, Sacramento, CA*, AIAA 2006-4324, American Institute of Aeronautics and Astronautics, Washington DC, 2006.

[9]P. W. Terry, Reviews of Modern Physics **72**, 109 (2000).

[10]G. Janes and R. Lowder, Physics of Fluids **9**, 1115 (1966).

[11]E. Ahedo, J. Gallardo, and M. Martínez-Sánchez, Physics of Plasmas **10**, 3397 (2003).

[12]J. Gallardo and E. Ahedo, On the anomalous diffusion mechanism in Hall thrusters, in *Proc. 29th International Electric Propulsion Conference, Princeton, USA*, IEPC-2005-117, Electric Rocket Propulsion Society, Fairview Park, OH, 2005.

[13]E. Ahedo, Physics of Plasmas **9**, 4340 (2002).

[14]J. J. Szabo, *Fully kinetic numerical modeling of a plama thruster*, PhD thesis, Massachusetts Institute of Technology, 2001.

[15]N. Meezan and M. Capelli, Physical Review E **66**, 036401 (2002).

[16]S. Barral, K. Makowski, Z. Peradzynski, N. Gascon, and M. Dudeck, Phys. Plasmas **10**, 4137 (2003).

[17]O. Batishev and M. Martínez-Sánchez, Charge particle transport in the Hall effect thruster, in *Proc. 28th International Electric Propulsion Conference, Toulouse, France*, IEPC-03-188, Electric Rocket Propulsion Society, Fairview Park, OH, 2003.

[18]E. Ahedo and F. Parra, Physics of Plasmas **12**, 073503 (2005).

[19]D. Sydorenko, A. Smolyakov, I. Kaganovich, and Y. Raitses, Physics of Plasmas **13**, 014501 (2006).

[20]E. Ahedo and V. de Pablo, Physics of Plasmas **9**, 083501 (2007).

[21]D. Sydorenko, A. Smolyakov, I. Kaganovich, and Y. Raitses, Physics of Plasmas **14**, 0134508 (2007).

[22]A. Antón, D. Escobar, and E. Ahedo, Contour algorithms for a Hall thruster hybrid code, in *42th Joint Propulsion Conference, Sacramento, CA*, AIAA-2006-4834, American Institute of Aeronautics and Astronautics,Washington, DC, 2006.

[23]D. Escobar and E. Ahedo, Improved electron formulation for a Hall thruster hybrid model, in *42th Joint Propulsion Conference, Sacramento, CA*, AIAA-2006-4326, American Institute of Aeronautics and Astronautics,Washington, DC, 2006.

[24]D. Escobar, A. Antón, and E. Ahedo, Simulation of high-specific-impulse and double-stage Hall thrusters, in *Proc. 29th International Electric Propulsion Conference, Princeton, USA*, IEPC-2005-040, Electric Rocket Propulsion Society, Fairview Park, OH, 2005.